ACADEMIA ROMÂNĂ
Revue Roumaine de Chimie
http://web.icf.ro/rrch/

Rev. Roum. Chim.,
2013, *58*(2-3), 239-249

Dedicated to Professor Bogdan C. Simionescu on the occasion of his 65th anniversary

SOL-GEL HYBRID NANOCOMPOSITES WITH OXIDE NANOPARTICLES

Luminita PREDOANA,[a] Mariuca GARTNER,[a] Valentin Serban TEODORESCU,[b] Madalina NICOLESCU,[a] Mihai ANASTASESCU[a,*] and Maria ZAHARESCU[a]

[a] "Ilie Murgulescu" Institute of Physical Chemistry of the Roumanian Academy
202 Splaiul Independentei, 060021 Bucharest, Roumania
[b] National Institute of Material Physics, 105 bis Atomistilor Street,
077125 Bucharest-Măgurele, Roumania

Received December 20, 2012

In the present work the influence of the method of preparation on the characteristics of sol-gel hybrid nanocomposites with oxide nanoparticles was studied. The chosen system consists of a SiO_2 matrix based on methyltriethoxysilane (MTEOS) and laboratory made TiO_2:CeO_2 (4:1) nanopowder. The doping of the matrix was realized either by dispersion of previously prepared binary nanopowder in the matrix solution or by *in situ* generation of the TiO_2-CeO_2 nanoparticles during the matrix hydrolysis-condensation processes. Films were deposited on silicon wafer and glass substrates by dip-coating method and were characterized as prepared and annealed at 120°C. The optical and morphological properties were determined by spectroellipsometry (SE), scanning electron microscopy (SEM), atomic force microscopy (AFM), their structural characterization was realized by IR spectroscopy and the thermal behavior was determined by thermogravimetric and differential-thermal analysis (TG/DTA). All characterization methods have shown that by the two preparation routes materials with different characteristics were obtained.

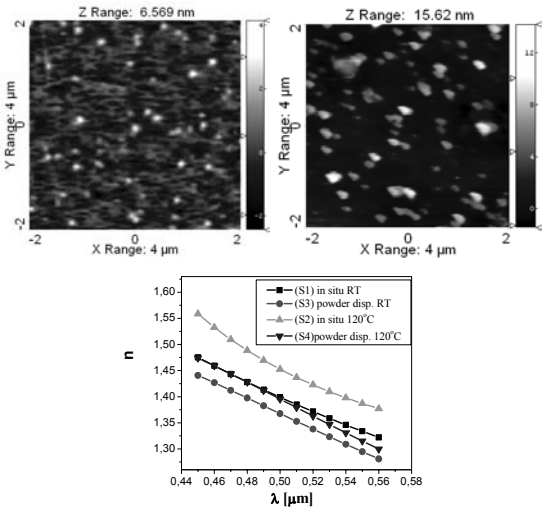

INTRODUCTION

According to the classification given by Sanchez[1] two types of hybrid materials could be prepared using sol-gel method. The class I-a refers to the hybrids in which no chemical bonds occur between the inorganic and organic components, while in the class II of sol-gel hybrid inorganic-organic materials, the organic and inorganic components are bonded by covalent bonds. These types of materials are obtained by hydrolysis-polycondensation of the organically modified alkoxides and the method of dopant introduction in the hybrid matrix plays a very important role on the material's final characteristics.

The most common precursors for the hybrid films preparation include: phenyl-trimethoxysilane (PTMOS), methyltriethisxysilane (MTEOS),

* Corresponding author: manastasescu@icf.ro

3-glycidoxypropyl-trimethoxysilane (GPTMS), trimethoxysilyl-propyl-methacrylate (TSPM), methylmethacrylate (MMA) and methacylic acid (MA)[2-14] as well as mixtures of organically substituted and un-substituted Si-alkoxides.[2-14]

Inorganic-organic hybrid materials belonging to class II, according to Sanchez's classification can offer multifunctionality and allow properties tailoring from subnanometer (atomic) to submilimeter (mesoscopic) length scales. The organic groups can modify the inorganic backbone by reducing the connectivity of the gel network allowing thick film deposition and lessening the processing temperature.

Films based on such materials could play a significant role in the field of micro- and nano-photonic devices (waveguides,[15-17] emitting devices,[18] quantum dot devices,[19] photonic band gaps and holographic materials[20]).

Doping the hybrid backbone with monocomponent and/or binary oxide powders is a well known procedure and could enhance the properties required for micro and nano-photonics but could in the same time add supplementary properties to the coatings as sensing, anticorrosive or catalytic ones. However, when the formation of the nanoparticles take place during the sol-gel process (class II of hybrids) and the post deposition thermal treatment is realized at low temperatures (below 150^0C) it is difficult to assume if there are only oxide particles formation or the precursors react also with the hybrid matrix and a mixed R-Si-O-Me-O-Si- oxide network is formed, as well. The embedment of the pre-synthesized oxides is a more sure way of knowing the composition of the particles introduced in a hybrid matrix. Functionalization of nanoparticles is in most of the cases necessary in order to hinder the aggregation of the previously prepared oxide particles and to improve their dispersability in the matrix or in the reaction medium. The problems concerning the homogeneity of the nanopowders embedment in hybrid matrix is more complicated when binary powders are under investigation.

In order to bring more information on the matter, in this work, the preparation of hybrid coatings in the R-SiO_2-(TiO_2-CeO_2) system by sol-gel method was studied. The system chosen consists of the methyltriethoxysilane (MTEOS) as SiO_2 matrix, considered as a model matrix, and TiO_2-CeO_2 powder in a TiO_2:CeO_2 = 4:1 ratio, used as dopant. The oxide powder was embedded in the hybrid material either by *in-situ* generation or by powder dispersion (without functionalization) and the thermal treatment of the coatings was realized at low temperatures, namely 120^0C. Such low temperatures of densification are of interest when hybrid films are deposited on aluminum based alloys used in aircraft fabrication, for corrosion protection and which are damaged at higher temperatures. The main objective is to establish a correlation between the method of embedment of the dopant particles in the system and the properties of the resulted films and gels.

The interest of using binary TiO_2-CeO_2 binary powders for doping a hybrid matrix is determined by the different application that such powders and films containing this oxides already have, as: catalysts,[21,22] materials for electrochromic devices,[23-28] oxygen sensors,[29] corrosion protection materials[2-14] and several other applications.[30-39]

EXPERIMENTAL

Powder and films preparation

The TiO_2-CeO_2 powder was prepared by the sol-gel method at a ratio of TiO_2:CeO_2 of 4:1 using $Ti(iOPr)_4$ (Aldrich) and $Ce(NO_3)_3{\cdot}6H_2O$ (Aldrich) as starting precursors in EtOH (Sigma-Aldrich) medium. The metal oxide powder preparation was achieved adding very low amount of NH_4OH 25% aqueous solution (Merck). All reagents were used as received, with no further purification. The resulted powder was filtered, washed with distilled water until complete removal of ethanol and secondary reaction products, dried in the oven for 48 h at 100^0C and then annealed 1 h at 400°C with a heating rate of 1°C/min in order to eliminate the water and organic residues. More details on the powders preparation were published previously in the paper.[40]

For films preparation a model system was chosen based only on methyltriethoxysilane. The composition and the experimental conditions for the matrix preparation are given in Table 1.

The oxide powder was embedded in the matrix solution either by *in situ* generation or by powder dispersion. In the last case the powder was first dispersed in alcohol by alternative mixing and sonication and then added to hybrid solution previously prepared. The mixed solution was kept under stirring for more 24 hours.

In the case of *in situ* particles' generation the matrix solution was previously prepared and mixed with the solution containing the TiO_2 and CeO_2 precursors, also previously realized. The experimental conditions are presented in Table 2.

Two types of solutions were prepared corresponding to the following molar composition: 90 mol% SiO_2-10 mol% (TiO_2-CeO_2) and 75 mol% SiO_2 - 25 mol % (TiO_2-CeO_2). In the case of the addition of oxide nano-powders previously prepared the highest concentration that allowed to obtaining stable suspension was of 90 mol% SiO_2-10 mol% (TiO_2-CeO_2) composition.

From the both type of solution prepared as mentioned above, thin films on glass and silicon wafer substrates have been deposited by dip-coating with a withdrawal rate of 5 cm/min. For all types of samples a thermal treatment of 30 min at 120 ^{o}C with a heating rate of 1°C/min was applied for film consolidation.

Table 1

Solution composition and experimental conditions for the SiO_2 matrix preparation

Sample	Metalic precursors	Molar ratios		pH	Experimental conditions		
		$\frac{ROH}{\sum \text{Precursors}}$	$\frac{H_2O}{\sum \text{Precursors}}$		T(°C)	t(h)	υ cP
SiO_2 matrix	CH_3-Si$(OC_2H_5)_3$	11	2	3	RT	24	2.14

Table 2

Starting solution and experimental conditions for in situ generation of the binary oxide nanoparticles

Sample	Metallic precursors	Molar ratios		pH	Experimental conditions	
		$\frac{ROH}{\sum \text{Precursors}}$	$\frac{H_2O}{\sum \text{Precursors}}$		T(°C)	t(h)
TiO_2:CeO_2 4:1	Ti(O-i$C_3H_7)_4$ $Ce(NO_3)_3.6H_2O$	35.6 R=-C_2H_5	3	5	RT	24

Characterization methods

The TiO_2-CeO_2 powder obtained in the conditions mentioned above was characterized by transmission electron microscopy (TEM) using a JEOL 200 CX microscope with a Topcon 00B instrument and by FT-IR spectroscopy using a Nicolete 6700 Spectometer and a resolution of 4 cm^{-1}.

X-ray diffraction investigation of the powder was realized with a Philips PW 1050 diffractometer with Bragg-Brentano geometry and Cu K_α radiation was used. The patterns have been scanned in steps of 0.02° (2θ) from 8° to 80° with a constant counting time of 30 s.

The dimension of the binary nanoparticles formed *in situ* was determined by Dynamic Light Scattering using a Zetasizer Nano-ZS ZEN 3600 from Malvern equipment.

The AFM experiments were carried out based on the Dynamic Force Module / Intermittent contact mode, using an EasyScan 2 model from Nanosurf® AG Switzerland. The phase contrast working mode was used for the samples imaging by means of a 10 μm x 10 μm high resolution scanner with vertical range of 2 μm, z-axis resolution 0.027 nm and a X-Y linearity mean error of less then 0.6%. The scan rate was around 1 Hz. The cantilever (NCLR type from Nanosensors™) was with spring constants of around 32 N/m and vibrating frequency of 166 kHz. Scanning Probe Image Processor (SPIP) program (v4.6.0.0) was used for image processing (tilt and bow correction) and root mean square roughness (RMS) calculation.

The optical and morphological properties of the films deposited on glass and silicon wafer were determined by spectroellipsometry (SE) and scanning electron microscopy. The optical parameters, the thicknesses and the porosities of the films have been determined by spectroellipsometry, performing measurements in the visible range (0.4 – 0.7 μm). The modeling of the spectroellipsometric spectra had been realized using Cauchy method of calculation for the samples deposited on silicon wafer and with the P-elipso program for the samples deposited on glass.

The modeling of the spectroellipsometric spectra had been realized using Cauchy method of calculation for the samples deposited on silicon wafer and with the B-EMA model[41] for the samples deposited on glass.

The structure of gel resulted by gelation of the solutions used for films deposition was determined by IR spectroscopy (see above) and its thermal behavior was established by thermodifferential and thermogravimetric analysis (DTA/TGA) using a Mettler Toledo TGA/SDTA 851e equipment with a heating rate of 5 °C·min^{-1}.

RESULTS AND DISCUSSION

In the literature hybrid coatings with complex compositions are usually prepared using several substituted siloxane precursors. The aim of this work was to obtain information about the influence of the nanopowder addition to such coatings, depending on the way of their preparation: *in situ* generation or by dispersion of the previously prepared nanopowders in the hybrid matrix. For this reason a simple system was chosen, based on the methyltrietoxisilane, considered as a model one.

Powder characterization

The as prepared powder using the conditions mentioned above was amorphous and had a light yellow color. By thermal treatment at 400^0C a structural ordering of the powders was noticed, although the vitreous character is still maintained. A complete description of the powder characteris-

tics was given in a previous paper.[40] Fig. 1 presents the TEM micrograph for the 80%TiO_2-20%CeO_2 powder thermally treated at 400°C.

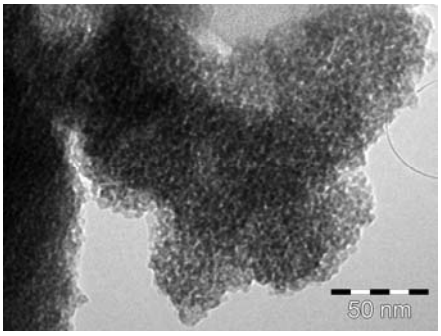

Fig. 1 – TEM micrograph for the 80%TiO_2-20%CeO_2 powder thermally treated at 400°C.

The binary oxide material is constituted from granular aggregates with sizes ranging between 50 and 100 nm, formed from crystallite of 2-3 nm. In the dried powder the aggregates have the tendency to agglomerate in larger structures. The vitreous character of the powders with the tendency to structural ordering was confirmed by the XRD results presented in Fig. 2, which show that the monoclinic $Ce_2Ti_2O_7$ compound starts to crystallize from the amorphous gel. The XRD results are very important as they confirm the reaction that took place during the sol-gel synthesis between the precursors, leading to formation of a binary powder not of a mixture of individual oxides.

The FT-IR spectrum of the binary oxide is presented in Fig. 3 and shows the following vibration bands: at ~ 510 cm^{-1} assigned the Ti-O bond, at ~ 600 cm^{-1} due to the Ti-O-Ti vibration superposed with the Ti-O-Ce cm^{-1}, at ~ 1630 cm^{-1} due to stretching vibration of the hydroxyl groups and ~ at 3400 cm^{-1}assigned to the elongation modes of the OH groups.[42]

The dimension of the particles obtained by *in situ* generation determined by Dynamic Light Scattering is presented in Fig. 4. As it can be observed a narrow particle size domain was obtained showing the formation of a very homogenous dispersion with particles between 1 – 3 nm.

Comparing the size of the two type of powders used in film preparation it is obvious that due to the difference in their size and aggregation tendency, their embedment will lead to different properties of the resulted films.

Coatings characterization

Using the experimental conditions presented above, in the case of *in situ* generation of the TiO_2-CeO_2 particles, adherent, homogeneous and continuous film was obtained as is shown by the SEM images (Fig. 5).

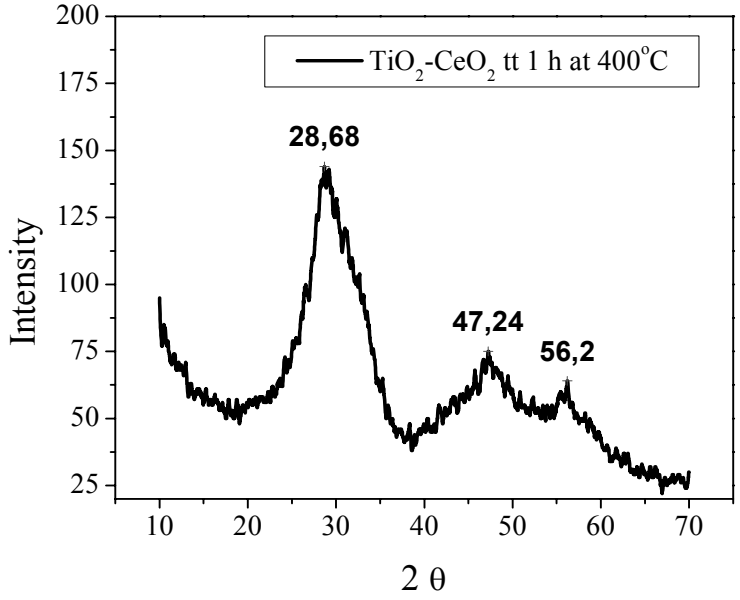

Fig. 2 – The XRD pattern for the TiO_2-CeO_2 powder thermally treated at 400°C.

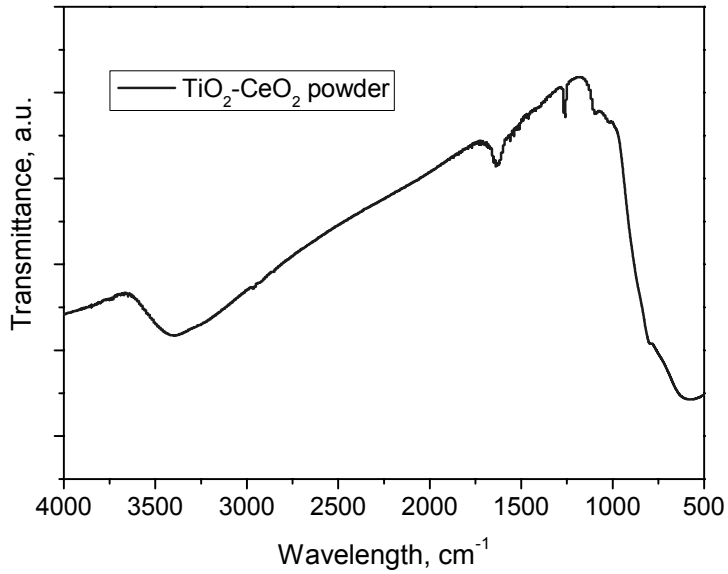

Fig. 3 – FT-IR spectra of the TiO_2-CeO_2 (80:20) powder thermally treated at 400 ^oC.

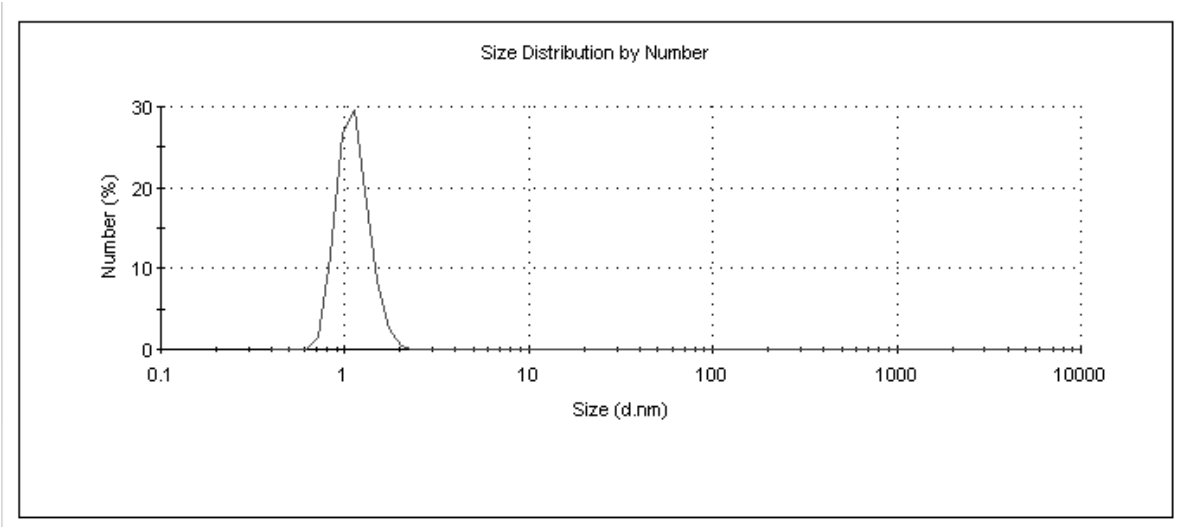

Fig. 4 – Particle size distribution by number for the *in situ* generation of nanoparticles in the hybrid matrix.

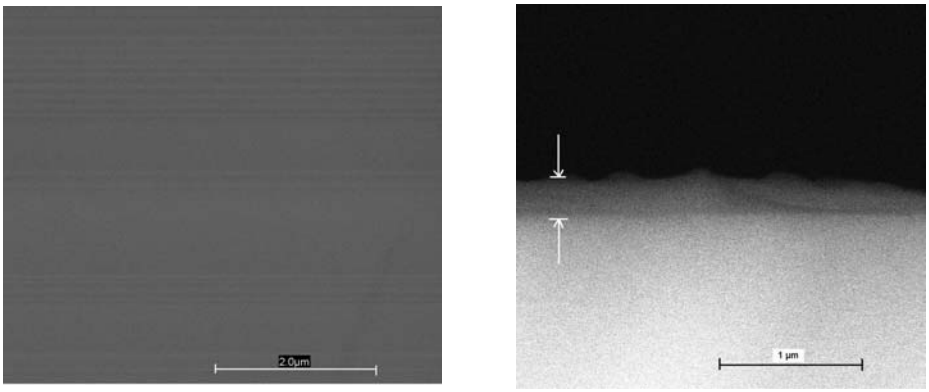

a) b)

Fig. 5 – SEM image of the R-SiO_2-TiO_2-CeO_2 film obtained by *in situ* generation of the oxide nanoparticles; a) plan view, b) cross section.

The SEM image (plane view) presents a homogeneous surface without cracks or porosity, while the thickness of the film determined by SEM on the cross section is around 250 nm.

The AFM images (three dimensional views) for both types of coatings deposited on Si wafer are shown in Fig. 6 presenting their surface morphology.

In the Fig. 6a the AFM image for the film obtained by *in situ* generation of the oxide nanoparticles is shown, confirming the low roughness of the film (RMS=0.59 nm).

In the case of the coatings obtained by dispersion of the previously prepared nanoparticles, without functionalization (Fig. 6b), a surface with a non-homogeneities could be observed that could be assigned to the nanopowder agglomeration in the hydrophobic hybrid SiO_2 matrix.

However, the roughness remains rather low (RMS=1.84 nm). On may suppose that using a more hydrophilic hybrid matrix, the dispersion of the previously prepared powder in the matrix will be improved. The assumption was confirmed by obtaining hybrid films based on a mixture of tetraethylorthosilicate (TEOS) and trimethoxysilyl-propyl-methacrylate (TSPM) doped with the same type of nano-powders which have shown a much lower roughness and a higher homogeneity,[43] as can be observed in Figure 7. In the later case, the roughness of the coating was 0.13 nm.

The refractive indices of the films deposited on silicon wafer and glass, calculated from the spectroellipsometric measurements, are presented in Figs. 8 and 9.

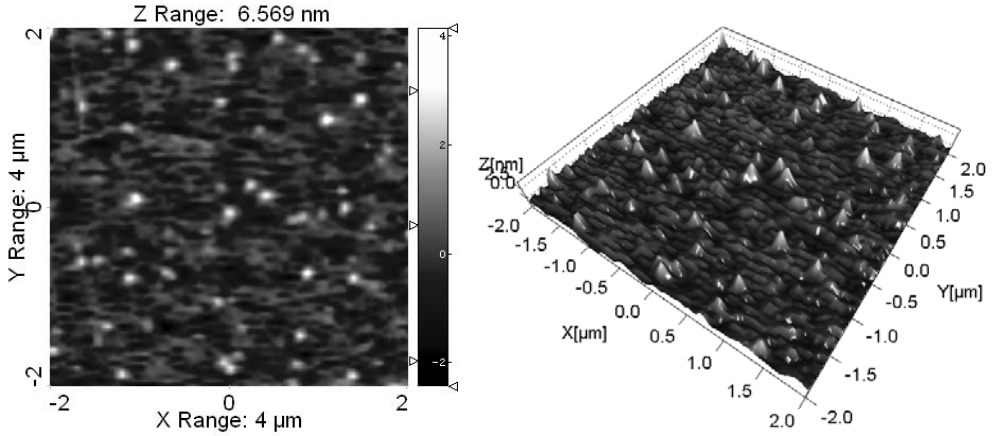

RMS=0.59 nm

(a)

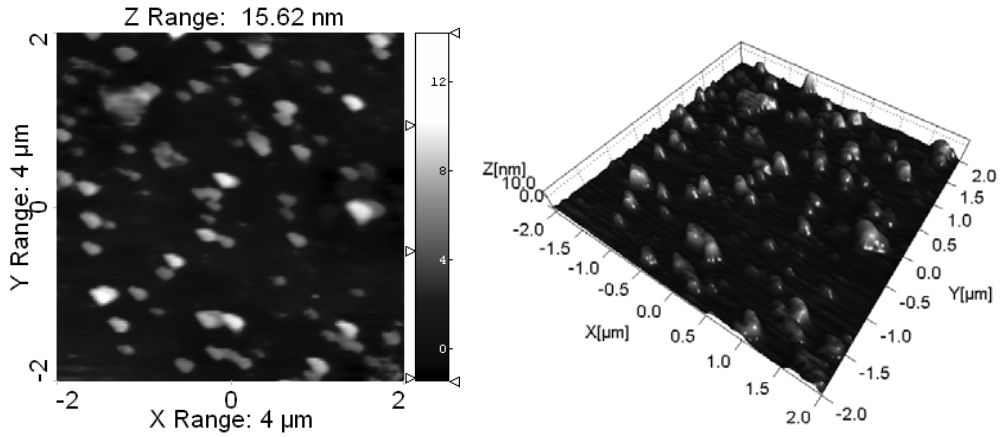

RMS=1.84 nm

(b)

Fig. 6 – AFM images (2D and 3D, topography) for the hybrid films deposited on Si wafer obtained by *in situ* generation of the oxides nanoparticles (a) and obtained by dispersion of the previously prepared nanoparticles (b).

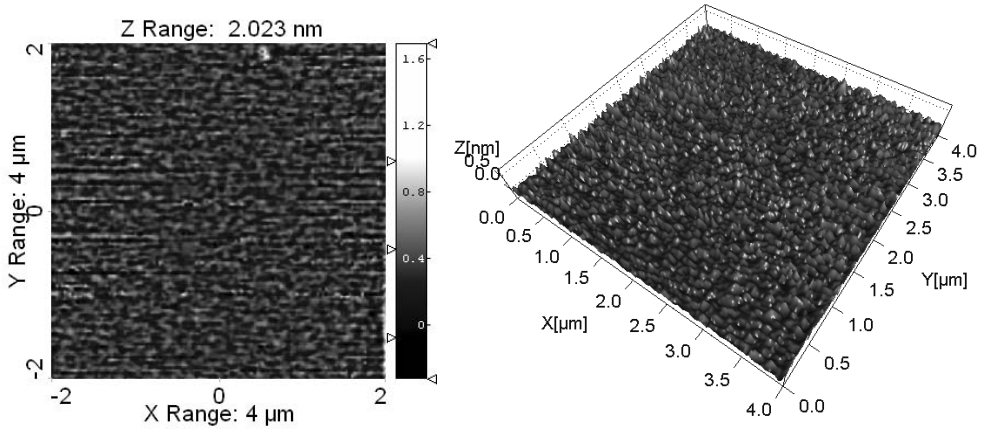

Fig. 7 – AFM images (2D and 3D, topography) of a tetraethylorthosilicate (TEOS) and trimethoxysilyl-propyl-methacrylate (TSPM)(65:35) based coating deposited on Si wafer using (TiO_2-CeO_2) particles previously prepared.

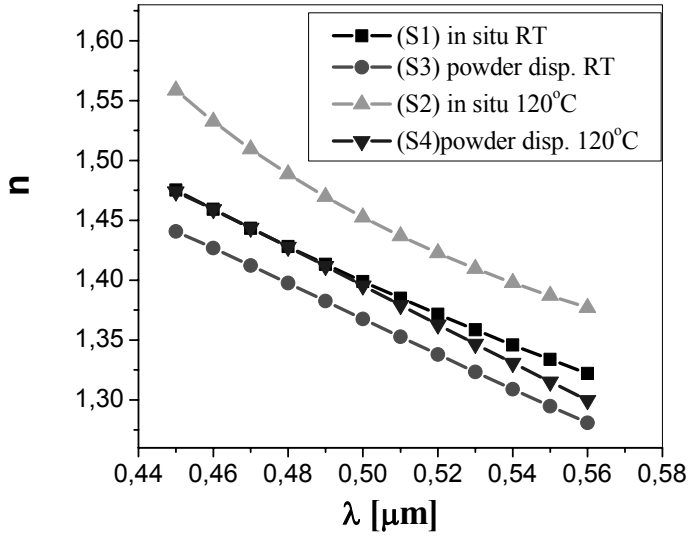

Fig. 8 – Refractive indices for the samples deposited on silicon wafer substrate.

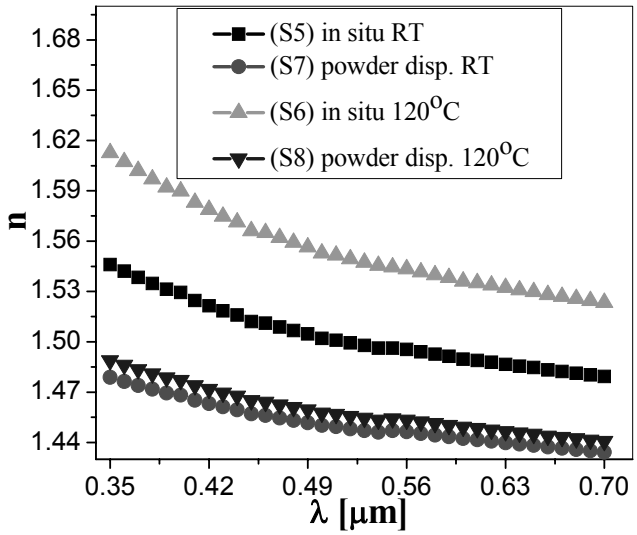

Fig. 9 – Refractive indices for the samples deposited on glass substrate.

Table 3

Spectroscopic results on the films depostited on Si wafer and glass substrate

Sample	Method	Thermal treatment (°C)	Film thickness d (Å)
Si wafer substrate			
S1	Particles *in situ* generation	-	2464
S2		120	2149
S3	Particles embedment	-	2246
S4		120	2236
Glass substrate			
S5	Particles *in situ* generation	-	2622
S6		120	2358
S7	Particles embedment	-	2467
S8		120	2462

Thickness of the films deposited on silicon wafer and glass substrate, calculated from spectroellipsometric measurements are presented in Table 3.

From the spectroellipsometric results and calculations, the following conclusions could be drawn:

- for the both types of substrates it can be observed that the films obtained from "powder dispersion" method exhibit lower values of the refractive indices in comparison with the one prepared by *in situ* method,
- for the same type of film it can be observed that the thermal treatment induces a small increase in the refractive indices values;
- for the films realized by *in situ* method, the thermal treatment induce a densification while for the films realized by "powder dispersion" no significant effect was noticed.

Films prepared from similar composition of sols[44] have shown different properties probably, due to their different thickness, determined by a different viscosity at the moment of deposition (not determined).

Gels characterization

Supplementary information on the synthesized compositions have been obtained by FT-IR spectroscopy measurements and DTA/TG analysis of the gels resulted by gelation of the suspension used for films deposition.

The IR spectra of the as prepared gels are presented in the Fig. 10, and the assignment of the vibration bands, according to the literature data[42, 45] are summarized in Table 4.

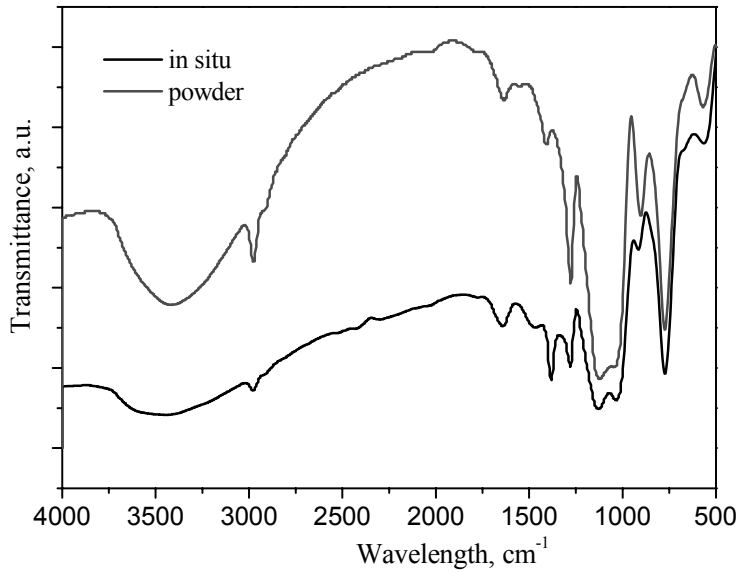

Fig. 10 – IR spectra of the R-SiO_2-TiO_2-CeO_2 (90:8:2) gels prepared *in situ* or by powder embedment.

Table 4

The bands assignment for the FT-IR spectra of the two gels

Wavelength (cm^{-1})	**Assignment**
600	Ti-O-Ti; (Ti-O-Ce)
780	ρCH_3; ν^{sym}(Si-O-Si)
900	Traces EtOH
1040	ν^{asym}(Si-O-Si)
1130	ν^{asym}(Si-O-C)
1280	δCH_3
1380	ν NO^{3-}
1410	δCH_2 from Si-CH_2-CH_2-Si
1640	δH_2O
2980	$\nu^{asym}CH_3$
3660 – 3746	νOH groups

It may by noticed that for the gel obtained by gelation of the suspension obtained by the dispersion of the pre-synthesized particles, a classical IR spectrum of MTEOS based gel is observed;[45] the presence of the (TiO_2-CeO_2) nanoparticles could be noticed only by the vibration bands at the about 600 cm^{-1}. For the gel obtained from the suspension obtained by *in situ* generation of the nanoparticles boarder vibration bands and with lower intensity were registered, underlying the formation of a more disordered Si-O-Si network. Supplementary vibration bands are also observed, as for example the band located at 1380 cm^{-1}, that could be assigned to ν NO^{3-} vibration.

This difference between the two spectra could be assigned to a more intense interaction between the matrix and the nanoparticles precursors in the case of their *in situ* generation.

The DTA/TGA results for the two types of gels are presented in Figs. 11 and 12.

On may notice that the decomposition is different in the studied samples.

The hybrid gel obtained by pre-synthesized oxide nanoparticles decomposes at 480^0C that is the temperature of undoped MTOS gel decomposition.[46,47] The weight losses at low temperatures could be assigned to the dehydration of the particles included in the hybrid matrix, without a strong interaction with the matrix.

For the gel obtained by *in situ* generation of the nano-particles a more complex decomposition curve is recorded and the decomposition of the hybrid matrix and burning out of the organics take place at temperatures with 100^0C higher than in the case when the previously prepared nanoparticles were embedded in the hybrid matrix. This fact could be correlated with the interaction between the precursors of particles generation with the silica matrix, leading to the formation of different molecular species with different but higher thermal stability.

Based on the results presented above on may conclude that in the case of the coating obtained by *in situ* generation of the particles and by thermal treatment up to only 120^oC and only 30 minutes plateau only the adsorbed water and the solvent is eliminate from the coatings, so that in the coatings composition several intermediate could be retained that could influence the coatings properties.

The discussed problem is complex and needs further investigations.

CONCLUSIONS

Sol-gel hybrid coatings with oxide nanoparticles deposited on silicon wafer and glass substrate have been successfully produced by both *in situ* generation and powder dispersion methods.

The sol-gel powder used for "powder dispersion" method proved to be in the nanometric scale and presents after a thermal treatment of 1 h at 400°C a tendency to crystallize in the $Ce_2Ti_2O_7$ monoclinic form. By *in situ* generation particles with smaller size were obtained, ranging between 1-3 nm.

The spectroellipsometric and AFM results revealed an important influence of the method of dopant generation on the film properties.

All characterization methods involved have shown that the two preparation routes led to materials with different characteristics. The dopant is clearly better dispersed in the hybrid matrix when their *in situ* synthesis method is involved but the byproducts from the nanoparticles generation reaction remain in the coating and could negatively influence its properties.

Future studies should include an optimization of the nanoparticles embedment in the hybrid matrix by powder functionalization and/or higher energetic dispersion methods (ultrasound finger, microwaves field).

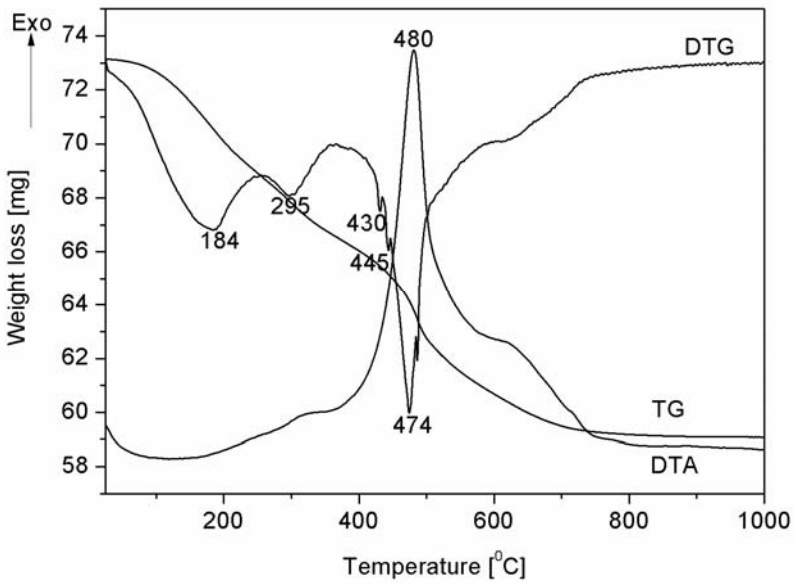

Fig. 11 – DTA/DTG curves for the hybrid gel prepared by powder embedment in the hybrid gel.

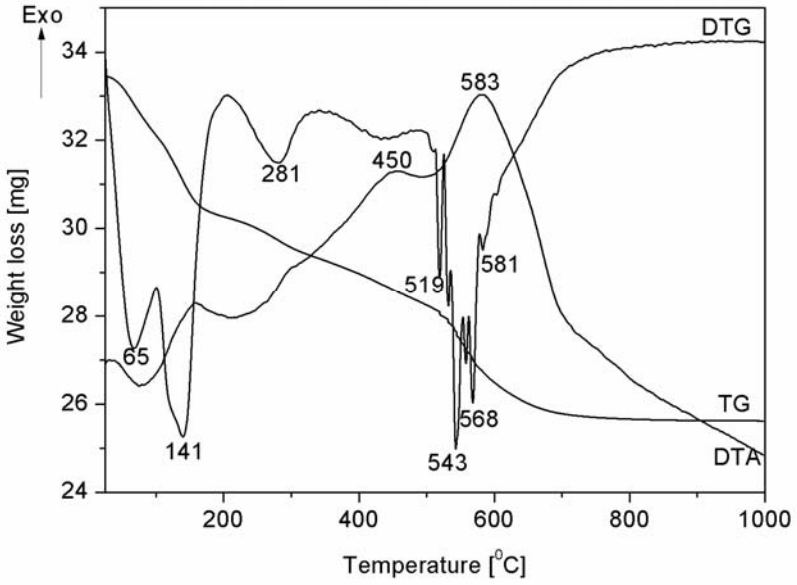

Fig. 12 – DTA/DTG curves for the hybrid gel prepared by *in situ* powder generation method.

REFERENCES

1. C. Sanchez and F. Ribot. *New J. Chem.*, **1994**, *18*, 1007.
2. A.R. Phani, F.J. Gammel, T. Hack and H. Haefke, *Mater. Corros.*, **2005**, *56*, 77.
3. R. Zandi-Zand, A. Ershad-langroudi and A. Rahimi, *Prog. Org. Coat.*, **2005**, *53*, 286.
4. R. Zandi-Zand, A. Ershad-langroudi and A. Rahimi, *J. Non-Cryst. Solids*, **2005**, *351*, 1307.
5. G.X. Shen, Y.C. Chen, L. Lin, C.J. Lin and D. Scantlebury, *Electrochim. Acta*, **2005***, 50*, 5083.
6. V. Nguyen, F.X. Perrin and J.L. Vernet, *Mater. Corros.*, **2004**, *55*, 659.
7. J. Gallardo, A. Duran and J.J. De Damborenea, *Corros. Sci.*, **2004**, *46*, 795.
8. M. Sheffer, A. Groysman, D. Starosvetsky, N. Savchenko and D. Mandler, *Corros. Sci.*, **2004**, *46*, 2975.
9. A. Pepe, M. Aparicio, S. Cere and A. Duran, *J. Non-Cryst. Solids*, **2004**, *348*, 162.
10. L. Fedrizzi, F.J. Rodriguez, S. Rossi, F. Deflorian and R. Di Maggio, *Electrochim. Acta*, **2001**, *46*, 3715.
11. N. Kumar, A. Jyothirmayi, K.R.C. Soma Raju and R. Subasri, *Ceram. Int.,* **2012**, *38*, 6565-6572.
12. E.D. Mekeridis, I.A. Kartsonakis and G.C. Kordas, *Prog. Org. Coat.,* **2012**, *73*, 142-148.
13. A. Wittmar, M. Wittmar, H. Caparrotti and M. Veith , *J. Sol-Gel Sci. Technol*., **2011**, 59, 621-628.
14. A. Wittmar, M. Wittmar, A. Ulrich, H. Caparrotti, and M. Veith, *J. Sol-Gel Sci. Technol*., **2012**, 1-13.
15. R.M. Almeida, *J. Non-Cryst. Solids*, **1999**, *259*, 176-181.
16. F. Rey-Garcia, C. Gomez-Reino, M.T. Flores-Arias, G.F. De La Fuente, A. Duran and Y. Castro, *Thin Solid Films*, **2011**, *519*, 7982-7986.

17. C. Molina, L.J.Q. Maia, Y. Messaddeq and S.J.L. Ribeiro, *Opt. Mater.*, **2012**, *34*, 910-914.
18. E. Cordoncillo, F.J. Guaita, P. Escribano, C. Phillippe, B. Viana and C. Sanchez, *Opt. Mater.*, **2001**, *18*, 309-320.
19. A. Schüler, M. Python, M. Valle del Olmo and E. De Chambrier, *Sol. Energy*, **2007**, *81*, 1159-1165.
20. I.G. Marino, D. Bersani and P.P. Lottici, *Opt. Mater.*, **2001**, *15*, 279-284.
21. S. Pavasupree, Y. Suzuki, S. Pivsa-Art and S. Yoshikawa, *J. Solid State Chem.*, **2005**, *178*, 128.
22. J. Rynkowski, J. Farbotko, R. Touroude and L. Hilaire, *Appl. Catal. A-Gen.*, **2000**, *203*, 335.
23. C.O. Avellaneda, L.O.S. Bulhoes and A. Pawlika, *Thin Solid Films,* **2005**, *471*, 100.
24. A. Verma, S.B. Samanta, A.K. Bakhshi and S.A. Agnihotry, *Solid State Ionics*, **2004**, *171*, 81.
25. D.L. Sun, S. Heusing, J. Puetz and M.A. Aegerter, *Solid State Ionics,* **2003**, *165*, 181.
26. F.E. Ghodsi, F.Z. Tepehan and G.G. Tepehan, *Electrochim. Acta,* **1999**, *44*, 3127.
27. C.O. Avellaneda and A. Pawlika, *Thin Solid Films*, **1998**, *335*, 245.
28. D. Keomany, J.P. Petit and D. Deroo, *Sol. Energ. Mat. Sol. C.*, **1995**, *36*, 397.
29. A. Trinchi, Y.X. Li, W. Wlodarsky, S. Kaciulis, L. Pandolfi, S. Viticoli, E. Comini and G. Sberveglirieri, *Sens. & Act.*, **2003**, *B95*, 145.
30. T. Lopez, F. Rojas, R. Alexander-Katz, F. Galindo, A. Balankin and A. Buljan, *J.Solid State Chem*., **2004**, *177*, 1873.
31. H. Zhu, Z. Qin, W. Shan, W. Shen and J. Wang, *J. Catal.*, **2004**, *225*, 267.
32. Z. Mei, W. Xidong, W. Fuming and L. Wenchao, *Sens. & Act.*, **2003**, *B92*, 167.
33. F.E. Ghodsi, F.Z. Tepehan and G.G. Tepehan, *Solar Energ. Mat. & Solar Cells*, **2001**, *68*, 355.
34. P. Knauth and H.L. Tuller, *Solid State Ionics*, **2000***, 136-137*, 1215.
35. G. Tavcar, K. Kalcher and B. Ogoreve, *Analyst*, **1997**, *122*, 371.
36. D. Camino, D. Deroo, J. Salardenne and N. Treuil, *Solar Energ. Mat. & Solar Cells*, **1995**, *639*, 349.
37. D. Keomany, C. Poinsignon and D. Deroo, *Solar Energ. Mat. & Solar Cells*, **1994**, *33*, 429.
38. A. Makishima, M. Asami and K. Wada, *J.Non-Cryst. Solids,* **1990**, *121*, 310.
39. A. Makishima, M. Asami and K. Wada, *J.Non-Cryst. Solids*, **1998**, *100*, 321.
40. M. Zaharescu, A. Wittmar, V. Teodorescu, C. Andronescu, M. Wittmar and M. Veith, *Z. Anorg. Allg. Chem.*, **2009**, *635 (12)*, 1915-1924.
41. D.A.G Bruggeman, *Ann. Phys. (Leipzig)*, **1935**, *24*, 636-679.
42. M. Palacio, P.I. Villabrille, G.P. Romanelli, P.G. Vasques and C.V. Caceres, *Appl. Catal. A-Gen.*, **2009**, *359*, 62-68.
43. M. Zaharescu, L. Predoana, A. Barau, D. Raps, F. Gammel, N.C. Rosero-Navarro, Y. Castro, A. Duran and M. Aparicio, *Corros. Sci.*, **2009**, *51[9]*, 1998-2005.
44. M. Zaharescu, M. Nicolescu, M. Gartner, A. Barau, L. Predoana, M. Anastasescu, M. Stoica and A. Szekeres, *J. Phys.: Conf. Ser.*, **2012***, 356 012018*, doi:10.1088/1742-6596/356/1/012018.
45. C.O. Avellaneda, L.O.S. Bulhoes and A. Pawlika, *Thin Solid Films*, **2005**, *471*, 100.
46. M. Zaharescu, A. Jitianu, A. Brăileanu, G. Pokol and J. Madarász*, J.Thermal Anal.Cal.*, **2001**, *64*, 689-696.
47. M. Zaharescu, A. Jitianu, A. Braileanu, V. Badescu, G. Pokol, J. Madarasz and Cs. Novak, *J. Therm. Anal. Cal.*, **1999**, *56*, 191.